Timing of consecutive traveling pulses in a model of entorhinal cortex

Anatoli Gorchetchnikov
Dept of Cognitive and Neural Systems,
Boston University,
677 Beacon St, Boston, MA 02215, USA
Email: anatoli@cns.bu.edu

Michael E. Hasselmo
Dept of Psychology,
Boston University,
64 Cummington St, Boston, MA 02215, USA
Email: hasselmo@bu.edu

***Abstract*— Previous work described a detailed spiking model of interactions between the hippocampus and entorhinal cortex in guiding rat spatial navigation behavior [1]. The timing of spiking activity in the entorhinal cortex is critical for the proper functioning of that model. Here we investigate the influence of several parameters of the model on the spike timing of consecutive traveling pulses within the network of spiking neurons with biologically realistic synaptic parameters. The results suggest that the local properties of the circuit consisting of pyramidal cell and interneuron affect the time interval between consecutive traveling pulses, while the strength of excitatory coupling between these circuits has little influence unless this strength is too small. These results can be generalized to other models of similar architecture that exhibit traveling pulses behavior, and also serve as a basis of further development of full scale realistic implementation of the formal model of spatial navigation [1].**

I. Introduction

In the model of spatial navigation by Hasselmo et al [1] the navigation task is solved by interaction between the knowledge about desired destination and knowledge about current location. This interaction takes place in hippocampal area CA1 using two converging inputs. The input from the hippocampal area CA3 represents the activity spreading forward along the path from the current location. The input from entorhinal cortex layer III (ECIII) represents the spread of activity from the goal location in the direction reverse to movement. The plots of neuronal activity illustrating the interaction between involved brain areas over a single theta cycle are presented in Figure 2. Numerical simulations showed that this mechanism allows the model to navigate successfully toward a known reward location, or visit several reward locations sequentially [2].

Implementation of this model with spiking neural network [3] led to conclusion that successful performance requires the arrival of spikes from two principal inputs, the hippocampal area CA3 and the layer III of entorhinal cortex within a narrow (about 15ms) time window from each other. Such precise timing requires full understanding of the influence of various parameters of the model on two time courses: interpulse interval between consecutive spikes of the same cell in ECIII (shown in Figure 2 by red arrow), and propagating of the activity through ECIII, ECII and CA3 (shown in Figure 2 by a set of blue arrows). Previously presented simulations used a set of biologically realistic parameters, which allowed the proper timing [3], but a detailed parametric study was not conducted. Here we concentrate on the timing of interpulse interval within the ECIII (red arrow in Figure 2).

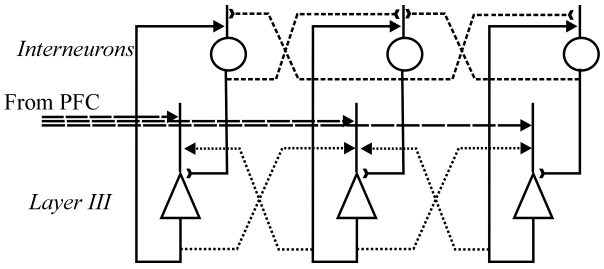

Fig. 1. Sketch of the connectivity within the model. Solid lines represent connections within a circuit for a single location; dotted lines – excitatory interactions between locations (only nearest neighbor connections are shown); dashed lines – inhibitory interactions between locations (weak); long-dashed lines – input projections. Arrowheads stand for excitatory synapses, archeads for inhibitory synapses.

To simplify the computation, in this study all populations of the original model [3] except ECIII were removed from the network. The resulting architecture of the ECIII is presented in Figure 1. Both pyramidal cells and interneurons are quiescent without input. Note, that in the case of constant external input to all pyramidal cells this model can be classified as a network of coupled neuronal oscillators, where each oscillator consists of a pair made up of pyramidal cell and interneuron. The properties of traveling pulses in this type of networks were studied by Ermentrout and Kleinfeld [4]. The model presented here has two significant differences, which might render the analysis in [4] inapplicable. Firstly, the coupling between the circuits is strong enough not to satisfy the definition of weak coupling from [4]. Secondly, there is no constant input to the circuits, and, therefore, they are only potential oscillators. Therefore, one can probably disregard the oscillatory nature of the circuit and collapse it into a single cell with long refractory period. The period of oscillations in the network of such cells was shown to scale linearly with the length of the refractory period [5], but traveling solutions were not investigated there.

In our full circuit model of spatial navigation [1] the input from prefrontal cortex to ECIII activates only the cells that correspond to goal locations. To replicate that, here the input

0-7803-7898-9/03/$17.00 ©2003 IEEE

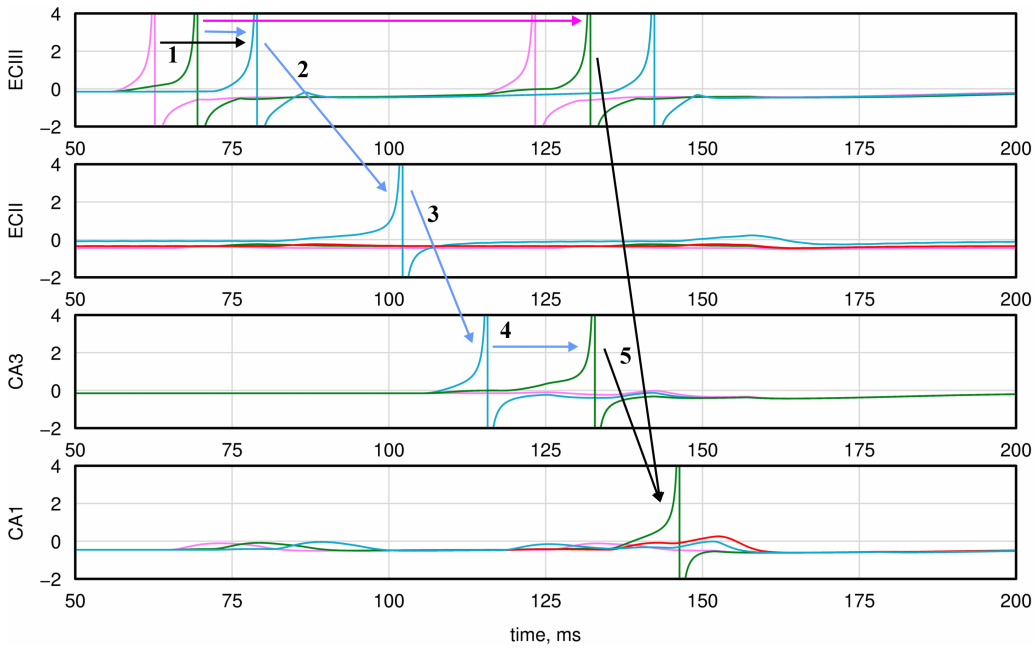

Fig. 2. Sketch of neuronal activity within a spiking model guiding the movement of a virtual rat during one step on the linear track. The animal starts two locations from the goal. Numbers next to arrows correspond to the following steps in the process. 1) The reverse spread of activity from the cell representing the goal location (cell activity in pink) through the cell representing the next desired location (cell activity in green) to the cell representing the current location (cell activity in blue). 2 and 3) Activation of the cell representing the current location in ECIII leads to consecutive activation of the cells representing the current location in ECII and CA3. 4) The forward spread of activity from current location in CA3. 5) Convergence between the forward spread and the second wave of the reverse spread leads to selection of the next desired location by the corresponding activity in CA1. Two time courses important for proper convergence are represented by blue and red arrows.

was limited to a single pyramidal cell, and this cell initiates the consecutive traveling pulses through the network. The activity spreads along excitatory connectivity between neighboring pyramidal cells, which follows the Gaussian profile. Therefore, the model falls within a class of networks with spatially decaying connectivity. Golomb and Ermentrout [6] analyzed the traveling solutions in this class of networks, but they studied the propagation of a single pulse and did not consider the interpulse interval, which is critical for our model of spatial navigation [1] and is the subject of this study.

II. Methods

The model uses the KDE Integrated Neuro-Simulation Software (KInNeSS) version 0.2.2alpha1[1], which allows the creation of the virtual environment for the model, and provides input from this environment in the form of depolarizing current injections to the respective input cells of the model. The environment was a horizontal linear track of length 14 and width 1 location/cell, surrounded by walls one location/cell thick to emulate a one-dimensional case.

Entorhinal neuronal populations in the model use two-compartmental cell representation with an output delay line representing the action potential traveling time through an axon. A population of neuronal elements representing prefrontal cortex provides the information about the goal location that initiates the traveling pulse in ECIII. These cells do not receive synaptic input, and, therefore, do not use dendritic compartment. The driving input was provided as a current injection to the prefrontal cell connected to the ECIII cell corresponding to the leftmost location on the track. Detailed descriptions of the compartments and parameters of the simulations are presented in the Appendix.

The first experiment consisted of multiple simulations where the strength of one-to-one inhibitory connections from interneurons to respective pyramidal cells varied from 1 to 10 with step 1 (in units corresponding to the density of synaptic channels, see Appendix), and the strength of excitatory connections between neighboring pyramidal cells varied as follows. The base profile was a Gaussian, scaled so that the peak value was equal to a numeric value from 1 to 10 with step 1 (called excitatory strength henceforth), and $\sigma = 0.6d$, where $d = 1$ for adjacent pyramidal cells. This profile was applied to the model by assigning the synaptic weights to connections between neighboring cells, with exclusion of the cell's projection to itself and all projections that had weight below 10^{-3}.

For each set of synaptic weights, the interspike intervals were recorded during 500 simulated milliseconds (3–10 spikes per cell depending on the parameters). The first four cells including the driving cell were excluded from the analysis to avoid the unstable pulses that occur close to the driving cell under some parameter settings. From the remaining ten cells all interspike intervals were combined in a sample (30–50 intervals per sample), and sample average, standard deviation

[1]Available for download at *http://temporal.bu.edu*.

and coefficient of variation were calculated.

In the second set of simulations the decay time constant of inhibitory synapse was varied from 6 to 8 ms with the step 0.2 ms, the excitatory and inhibitory connection strengths were fixed at 6 and 8, respectively. As a reference point for this experiment the dependency of intrinsic frequency of single uncoupled oscillatory circuit (pyramidal cell and corresponding interneuron) henceforth called local circuit frequency was measured for the same values of time constant. Since the local circuit frequency depends on the injected current, the current amplitude was adjusted to provide interspike intervals similar to these received in the network simulations.

Finally, the dependency of local circuit oscillatory frequency on the inhibitory strength was measured in an isolated circuit for two values of injected current, also adjusted to provide interspike intervals similar to the ones received in previous experiments.

III. Results

The results of the first simulation are summarized in Figure 5. The plateau of almost constant interpulse intervals for the strong local interneuron-to-pyramidal inhibition (panel A) together with lower standard deviation and coefficient of variance in the same parameter ranges (panels B and C) can be of critical importance for learning in the networks of similar architecture.

In some cases the excitation was strong enough to allow the spread of the activity to the cells corresponding to locations inside the walls of the environment. These cases were disregarded for three reasons. Firstly, the spread within the walls of the environment violated the emulation of one-dimensional setting and caused a pattern of network activation that differed from all presented in Figure 5 cases and, therefore, should be analyzed separately. Secondly, in the model of spatial navigation [3] the spread of activity in restricted locations like the walls renders the model inoperable. Finally, in two-dimensional case the domination of excitatory strengths over inhibitory strengths leads to seizure-like oscillatory solutions instead of traveling pulse solutions. Simulations that expressed such behavior were terminated as soon as the excessive spread of activity happened, and the respective data is omitted from Figure 5.

All runs with the excitatory strength of 1 were disregarded, since no traveling pulses were generated at this level of excitation. For low excitation (strength 2 and 3, left back part of the plot), the generation of next pulse often happened before the previous one moved far enough along the network. This led the network to skip the second pulse occasionally, and, therefore, to longer interspike intervals and higher variability of these intervals.

The results of the second and third simulations are plotted in Figures 3 and 4, respectively. The local circuit frequency in Figure 3 and the interval between consecutive traveling pulses in Figure 4 are plotted on the same graphs, but can only be used for the reference, since the experimental settings were different for these measurements. In both plots the error

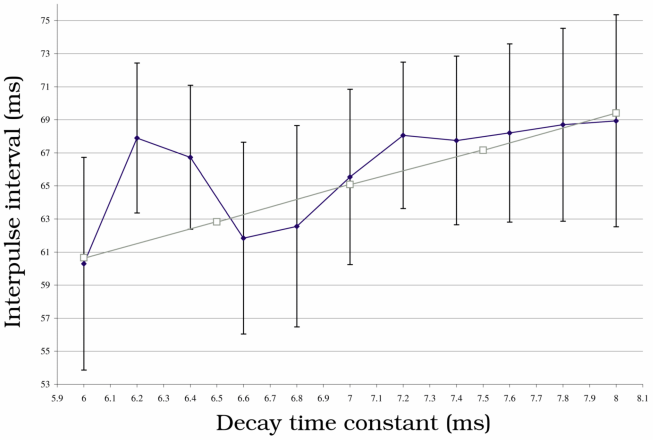

Fig. 3. Interval between consecutive traveling pulses as a function of the decay time constant of inhibitory synapse is shown in blue. For the reference, the gray line indicates the dependency of local circuit oscillatory frequency on the decay time constant.

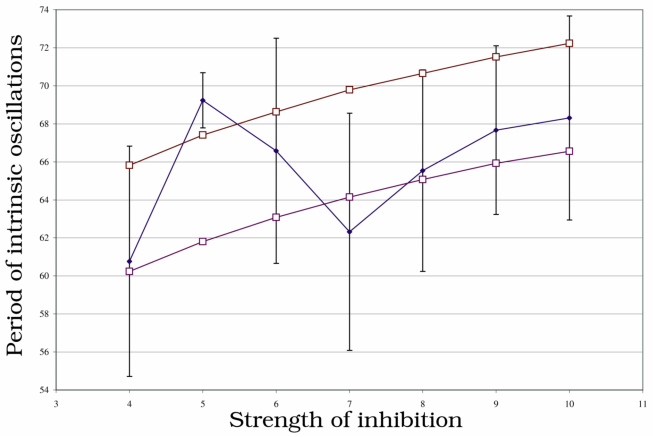

Fig. 4. Circuit intrinsic oscillatory frequency as a function of the strength of inhibitory connection. Two values of input current are plotted in red, the higher plot corresponds to the smaller value of the current. For the reference, the blue plot indicates the dependency of interval between consecutive traveling pulses on the strength of inhibitory connections.

of local circuit frequency measurements was negligible and mostly due to the discretization error, therefore it is omitted from the plots.

IV. Discussion

We investigated the influence of several parameters on the interpulse interval of consecutive traveling spikes in the network sketched in Figure 1 looking for the parameter ranges where the interspike interval stays approximately constant. As shown in Figure 5, such parameter regime exists and spans over wide range of medium to high strength of excitatory connections between pyramidal cells in Figure 1 as long as the strength of inhibitory connections from interneurons to pyramidal cells is high enough. This regime will be referred to as “persistent” in the following discussion.

The network can also be in two other regimes. One is the seizure-like oscillatory activity that occur when the level of

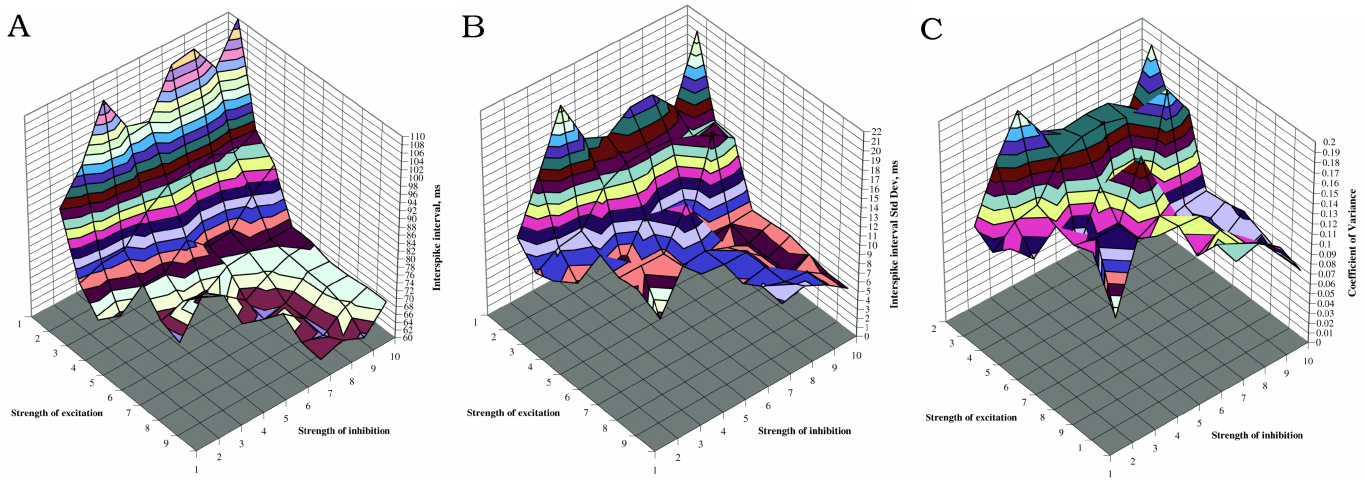

Fig. 5. Interval between consecutive traveling pulses as a function of the strength of inhibitory and excitatory connections. Inhibitory strength is on X axis, excitatory strength on Y axis. Missing front corners in each panel correspond to cases when the excitation is too strong compared to inhibition (see text). Panel A – average interspike interval; note the flattening of the plot for strong inhibitory values. Panel B – standard deviation of the interspike interval; note that it is the lowest for the flat part of panel A. Panel C – coefficient of variation; note that it is also the lowest for the flat part of panel A.

excitatory strength is too high comparing to the inhibition. In this partameter range traveling solution does not exist, and the results were omitted from Figure 5 to avoid confusion. The last regime (henceforth called "volatile") exists at low levels of excitatory connection strengths and shows as a ridge in panel A of Figure 5.

The difference in behavior between persistent and volatile regimes resulted from the relation between the wave speed and local circuit frequency. In the volatile regime, the wave speed was slower than the local circuit frequency (or the refractory period of the circuit), which led to the attempt to generate a new wave before it could spread without collapsing on the previous wave. This led to occasional skipping pulses during the simulations as well as to strong dependency of the interpulse interval on the strength of excitation (through its influence on the wave speed). For high values of excitation strength the wave speed was faster than the refractory period, therefore the latter controlled the interpulse interval leading to persistent regime as discussed below.

The dependency of the interspike interval on the decay time constant of the inhibitory synapse appears to follow a similar trend to the dependency of local circuit frequency for the pair consisting of pyramidal cell and interneuron. This similarity suggests that the local circuit frequency at least in part determines the interspike interval in the model. The local circuit frequency scales linearly with the decay time constant both in our numeric simulations presented here and in theoretical analysis of similar circuits [5]. The interpulse interval in Figure 3 appears to saturate, but more data is necessary to determine whether it is a significant trend.

The dependency of local circuit frequency on the strength of inhibition follows the exponential decay due to the dual exponential synaptic implementation in the model. The interpulse interval follows a similar trend (see Figure 4). Together, the results plotted in Figures 3 and 4 suggest that the local

TABLE I

LOCAL CIRCUIT OSCILLATION PERIOD AS A FUNCTION OF INHIBITORY STRENGTH IN ISOLATED CIRCUIT.

Inhibitory strength	0	0.1	1	5	10
Period, ms	31.2	35.7	55.6	66.1	71.4

properties of the circuit consisting of pyramidal cell and interneuron are the major factor that determines the interpulse interval when the model is in persistent regime[2].

The increase of inhibitory connections strength within the local circuit influences the interpulse interval through the change of local circuit frequency described above. Note that only the slow changing tail of this exponent falls into the range of inhibitory strengths studied here. Lower values of inhibitory strength showed much higher influence on local circuit frequency, when the isolated circuit was studied (see Table I), but they also led the network into epilepsy-like oscillatory behavior instead of traveling pulse solutions, when these circuits were combined together. Therefore, in the network the increase of inhibitory strength leads only to a minor increase in interspike interval between consecutive traveling pulses.

A more important effect of the inhibitory strength increase in the studied range is the stabilization of interpulse interval for a range of excitatory strengths. The width of this range increases with the strength of inhibition, as shown in Figure 5 and creates the persistent regime. Note that not only the interpulse interval becomes approximately constant (light blue flat part of the panel A towards the right back of the panel), but also the variance became smaller in this parameter regime

[2]This is only true, if the driving input is either constant current or very high frequency (much higher than the local circuit frequency) low amplitude stimulation used in simulations presented here. Low frequency stimulation will affect the interpulse interval by driving the activity in the network.

(panels B and C). Stabilized timing in the network over the range of excitatory strengths can allow better learning in the network, since the modification of the excitatory connections and redistribution of the network activation will not cause disruption of the overall timing of the network activity, and, therefore will reduce any negative effect learning can induce on communication between populations in the network.

Applying these results to the model of spatial navigation [1], one can conclude that the balance of excitatory and inhibitory strengths should not matter much for the behavior of the model as long as both strengths stay not lower than 4. In this case the interspike interval falls mostly within 60–70ms. The actual simulations of [3] used 4 and 5 for excitatory and inhibitory strengths, respectively, and showed that this interval allows proper behavior. The results from Figure 5 show that a wide variety of parameter settings can achieve a similar interval. Out of this variety the strongest inhibition is preferable if learning is enabled in the excitatory lateral connectivity of the model.

ACKNOWLEDGMENTS

This research was supported by NIH grants MH60013, MH61492, MH60450, and DA16454.

APPENDIX

A. Dendritic compartment

Dendritic compartment representation is derived from the standard approximation of the cable equation [7]:

$$C_m \frac{dV_m}{dt} = \sum_{Ch} g_{Ch}(E_{Ch} - V_m) + g_a(V_{m+1} + V_{m-1} - 2V_m) - g_l V_m \quad (1)$$

where V_m is a membrane potential in this compartment $[mV]$, $V_{m\pm1}$ are membrane potentials in neighboring compartments $[mV]$, g_{Ch} is a conductance of ligand gated ion channel $[mS]$, g_l is a leakage conductance $[mS]$, g_a is an axial conductance $[mS]$, and C_m is a membrane capacitance $[\mu F]$.

Equation (1) can be simplified for the purpose of this study to

$$C_m \frac{dV_m}{dt} = \sum_{Ch} g_{Ch}(E_{Ch} - V_m) + g_a(V_{m+1} - V_m) - g_l V_m \quad (2)$$

since there is only one neighboring compartment. Further more, to convert the actual capacitance and conductances to their dimension independent counterparts, we divide both sides by πdl to obtain

$$C_M \frac{dV_m}{dt} = \sum_{Ch} \frac{g_{Ch}}{\pi dl}(E_{Ch} - V_m) + \frac{dg_A}{4l^2}(V_{m+1} - V_m) - g_L V_m \quad (3)$$

where $C_M = 1\mu F/cm^2$. Current version of KInNeSS allows to set

$$z = \frac{dg_A}{4l^2}\left[\frac{mS}{cm^2}\right] \quad (4)$$

directly.

For the ligand-gated channels, the value $\sum_{Ch} \frac{g_{Ch}}{\pi dl}$ is represented as individual channel conductances $g_{Ch}[nS]$ times the synaptic weight $w = \frac{N_{Ch}}{\pi dl}\left[\frac{10^6}{cm^2}\right]$ corresponding to a channel density in millions of channels per cm^2 of the membrane. Channel conductance is calculated according to a dual-exponential equation

$$g_{Ch} = \frac{\bar{g}_{Ch} p}{\tau_f - \tau_r}(e^{-\frac{t}{\tau_f}} - e^{-\frac{t}{\tau_r}}) \quad (5)$$

if $\tau_f \neq \tau_r$, and according to the alpha function

$$g_{Ch} = \bar{g}_{Ch} \frac{t}{\tau_f} e^{(1-\frac{t}{\tau_f})} \quad (6)$$

if $\tau_f = \tau_r$. In both cases $\bar{g}_{Ch}[nS]$ is the maximal conductance, and t is time since presynaptic action potential. In (5) p is a scaling coefficient that enforces

$$\max\left(\frac{p}{\tau_f - \tau_r}(e^{-\frac{t}{\tau_f}} - e^{-\frac{t}{\tau_r}})\right) = 1 \quad (7)$$

Note that setting of the synaptic weight w to a experimentally measured channel density in the synapse would not be correct. It should accommodate the non-uniform distribution of ligand-gated channels in the compartment by averaging out the total number of channels in respective synapses over the membrane area of a *whole* compartment, not just the area of the synapse.

B. Somatic compartment

To lower the computational complexity of the model, the generation of action potentials is simulated using the reduced version of Hodgkin-Huxley equation also known as the theta-neuron or canonical Type I equation [8], [9]. This equation was modified to take the form

$$\begin{cases} \frac{d\theta}{dt} = [1 - \cos(\theta) + (1 + \cos(\theta))(qI - r)]\tau & \text{if } \theta \leq 3.125 \\ \theta = -3.04 & \text{otherwise} \end{cases} \quad (8)$$

where the numerical limits for θ were set so that membrane potential

$$V_m = \tan\left(\frac{\theta}{2}\right) \quad (9)$$

changes between approximately -20 and 120 mV. This allows us to replace the reduced representation with a complete Hodgkin-Huxley type equation without affecting the rest of the model if the need arises. The dimensionless parameter r is the original threshold controlling the dynamics of the cell. In the absence of input, the negative value of r sets the cell in excitable state, when a certain excitatory input is necessary to make it fire, while a positive value of r sets the neuron to a constantly firing state, when the excitatory input only modifies the firing frequency, but the inhibitory input can force it to cease firing. For more detailed discussion of this parameter influence see [9].

Additional modifications over the original version of reduced equation discussed in [9] include two dimensionless

TABLE II

POPULATION-SPECIFIC PARAMETERS OF THE MODEL.

Population	$\bar{g}_{AMPA}$, nS	r	Axonal delay, ms
Prefrontal cortex	n/a	-0.01	0.1
EC III interneurons	0.15	-0.01	0.1
EC III pyramidals (from PFC) (recurrent)	 0.247 0.15	-0.02	2.0

TABLE III

CONNECTION STRENGTHS.

Target	Type	Source	Weight(σ)
EC III interneurons	AMPA GABA	EC III pyr recurrent	9.0 0.25 (0.8)[a]
EC III pyramidals	AMPA	PFC	1.0 (0.6)

[a]Recurrent projections exclude the connection from cell to itself.

scaling factors: q – overall voltage gain factor that allows scaling of realistic synaptic potentials provided by (3) to values fit for use by (8); τ – time scaling factor that allows to adjust behavior of (8) to the same timescale as the rest of the model.

The input current is calculated according to a simplified version of the second term in (3)

$$I = zV_{m-1} \tag{10}$$

Comparing to (3) $V_m = 0$ here, because due to the specific nature of the reduced representation, the value of V_m stays within $[-0.6, 0.6]\ mV$ unless the spike is generated (in which case the influence of the input on the cell dynamics is minimal), while the value of V_{m-1} is of the order of tens mV. Parameter z is defined in (4).

C. Parameters of the simulations

For simplicity, all of the populations use only two types of synaptic channels: AMPA receptor and GABA_A receptor with the parameters as described in [10]. Unless the parameter was under study in specific experiment, the following values were used. For AMPA channels $E_{Ch} = 0mV$, $\tau_r = 2ms$, $\tau_f = 2ms$, $\bar{g}_{Ch}$ varied from population to population and is listed in Table II. Parameters for $GABA_A$ channels were $E_{Ch} = -70mV$, $\tau_r = 1ms$, $\tau_f = 7ms$, $\bar{g}_{Ch} = 2.461nS$. Parameters in equation (8) were: $q = 10$, $s = 0.45$, and threshold r was population specific and is listed in Table II.

KInNeSS does not allow to set different axonal delays for different outputs of the same cell. To compensate for this problem, the axonal delay for pyramidal cells was set to the pyramidal-to-pyramidal value, and axonal delay of the interneurons was artificially reduced to accommodate smaller pyramidal-to-interneuron delay. The axonal delay of prefrontal cells does not influence the system dynamics, since they do not receive any recurrent input. In equations (3-4) for simplicity $z = 3.0$ and $g_l = 0$ for all cells. Synaptic connection strengths that did not change across experiments are listed in Table III.

REFERENCES

[1] M. E. Hasselmo, J. Hay, M. Ilyn, and A. Gorchetchnikov, "Neuromodulation, theta rhythm, and rat spatial navigation," *Neural Netw*, vol. 15, no. 4-6, pp. 689–707, 2002.

[2] A. Gorchetchnikov and M. E. Hasselmo, "A model of hippocampal circuitry mediating goal-driven navigation in a familiar environment," *Neurocomputing*, vol. 44-46, pp. 423–427, 2002.

[3] ——, "A model of septal, entorhinal and hippocampal interactions to solve multiple goal navigation tasks," *Soc Neurosci Abstr*, vol. 32, p. 676.16, 2002.

[4] G. B. Ermentrout and D. Kleinfeld, "Traveling electrical waves in cortex: Insights from phase dynamics and speculation on a computational role," *Neuron*, vol. 29, no. 1, pp. 33–44, 2001.

[5] R. Curtu and G. B. Ermentrout, "Oscillations in a refractory neural net," *J Math Biol*, vol. 43, pp. 81–100, 2001.

[6] D. Golomb and G. B. Ermentrout, "Effect of delay on the type and velocity of travelling pulses in neuronal networks with spatially decaying connectivity," *Network: Comput Neural Syst*, vol. 11, pp. 221–246, 2000.

[7] J. B. Bower and D. Beeman, *The Book of GENESIS. Exploring Realistic Neural Models with the GEneral NEural SImulation System*. New York: Springer-Verlag, 1995.

[8] G. B. Ermentrout and N. Kopell, "Parabolic bursting in an excitable system coupled with slow oscillation," *SIAM J Appl Math*, vol. 46, pp. 233–252, 1986.

[9] F. C. Hoppensteadt and E. M. Izhikevich, *Weakly Connected Neural Networks*. New York: Springer-Verlag, 1998.

[10] E. Fransen, A. A. Alonso, and M. E. Hasselmo, "Simulations of the role of the muscarinic-activated calcium-sensitive nonspecific cation current i_{NCM} in entorhinal neuronal activity during delayed matching tasks," *J Neurosci*, vol. 22, no. 3, pp. 1081–1097, 2002.